Reaction between Iron-alloy and Mantle Minerals in the Presence of Sulfur: Implication for the Earth's Core Formation

T. Uchida, Y. Wang, M. L. Rivers, S. R. Sutton
GeoSoilEnviro Consortium for Advanced Radiation Sources (GSECARS),
The University of Chicago, Chicago, IL, U.S.A.

Introduction

The Earth's core consists of a liquid outer core and a solid inner core [1], which geophysical and cosmo-chemical evidence [2, 3] indicate are made predominantly of iron (Fe) However, there is a mismatch between the density of the core and density of pure iron at corresponding pressures (*P*) and temperatures (*T*). The liquid outer core is about 10% less dense than pure iron, while the solid inner core may be as dense as pure iron. This mismatch is ascribed to the presence of light elements [2]. Results from a recent high-*P* and high-*T* experiment support the notion [4] that light element(s) must be present in the inner as well as the outer core on the basis of the newly estimated thermal expansivity of pure iron [5].

The nature of the light elements in the cores is strongly linked to the core formation process. So far, S, H, C, Si, and O have been considered candidate elements, but there has been no consensus on which one is most predominant because of the lack of knowledge about this portion of the Earth [6]. The research discussed here examines the effects of sulfur as a predominant light element in the Earth's core. Several experiments have been conducted with a variety of surrounding mantle materials (MgO, Mg_2SiO_4, and $MgSiO_3$) at between 4 and 16 GPa by using the DIA and the T-cup multi-anvil high-pressure modules.

Methods and Materials

High-*P* and high-*T* *in situ* x-ray experiments were performed by using the 250-ton press installed at the GSECARS 13-BM-D beamline at the APS, with either a cubic-anvil DIA or split-cylinder T-cup high-pressure module. *In situ* x-ray diffraction measurements were carried out on the basis of the energy-dispersive method with an energy range of 20-130 keV. Figure 1 shows the schematics of the x-ray diffraction and imaging setup. For x-ray diffraction, the incident x-ray beam is collimated by the front slits (100×100 μm), and diffracted X-rays are detected by a Ge solid-state detector (SSD) at a fixed diffraction angle of 6°. For x-ray imaging, an aluminum attenuator (10-mm thick) replaces the front slits. This helps us enlarge the beam size (3×3 mm) and control the beam intensity to optimize the image contrast. Transmitted x-rays are converted by the YAG single crystal into visible light, which is then reflected by the mirror through a microscope objective into the charge-coupled device (CCD) camera. Diffraction and imaging modes can be interchanged by driving the incident slits in (for diffraction) and out (for imaging) of the x-ray beam path.

Mechanically homogenized starting materials, summarized in Table 1, were compressed to high *P* and then heated until melting occurred. While the sample was being heated, the x-ray image and diffraction pattern were taken at each *P* and *T* condition.

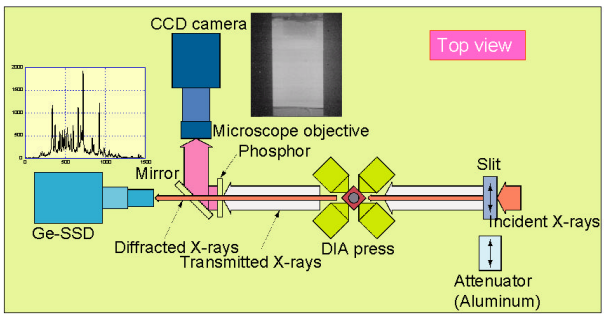

FIG. 1. X-ray diffraction and imaging setup (top view) for DIA experiments. For T-cup experiments, the virtual goniometer of the SSD is inclined by 35.2° from the vertical plane because of the geometry of second-stage anvils. Diffracted x-rays go above the YAG single crystal and mirror assembly and are then detected by a Ge SSD. The YAG phosphor enables us to "see" inside the cell by using the CCD camera. The imaging mirror is small and far enough from the press so that it does not conflict with the diffraction assembly.

Table 1. Starting materials and experimental conditions.

Run No.	HP module	Mantle mineral	Fe:FeS_2: mantle mineral[a]	Pressure (GPa)	Temp. (K)
D0319	DIA	$MgSiO_3$	5:1:6	4	1250
D0320	DIA	Mg_2SiO_4	5:1:6	4	1300
D0321	DIA	MgO	5:1:6[b]	4	1050
T0317	T-cup	$MgSiO_3$	5:1:6	16	1100
T0279	T-cup	Mg_2SiO_4	5:1:6	16	1400
T0257	T-cup	MgO	5:1:6	16	1100

[a] Mixing ratio is represented by weight.
[b] Pure Fe includes 33% of large grain powder.

Results and Discussion

Figure 2 shows the diffraction-pattern change during the heating cycle for the system Fe-FeS_2-MgO. Pyrite (FeS_2) starts reacting with Fe at 700K. At the same time, both MgO and Fe (with body-centered cubic [bcc] structure) peaks shift toward low energy, indicating the expansion of lattice parameters with the same structure. Then *a*-Fe transforms to the *g* (face-centered cubic [fcc]) phase at 800K. Above 1000K, both Fe and FeS (with NiAs structure) peaks disappear, indicating melting. A comparison of the diffraction patterns before and after the experiment shows significant shift of Fe and MgO peaks (Fig. 3). When it is assumed that the lattice parameter of wüstite is expressed as a linear function of Fe content (Fig. 4), the peak shift of MgO can be explained by Fe incorporating into the oxide and forming magnesiowüstite. From the lattice parameters, we could estimate that 20% of the Fe (in molar ratio) is contaminated in magnesiowüstite.

Figure 5 shows the diffraction-pattern change for the system Fe-FeS_2-Mg_2SiO_4 while the sample was being heated. In contrast with the MgO system, Mg_2SiO_4 peaks remained unshifted even when FeS_2 reacted with Fe. After the experiments, the Mg_2SiO_4 peaks returned to the original positions (Fig. 6). The system containing $MgSiO_3$ shows the same feature (Fig. 7). Thus, both olivine and enstatite are inert with Fe and FeS, with no clear evidence of any reaction. Because the pressure and temperature conditions as well as the sample chamber materials were similar to those used in the MgO-containing sample, the difference must be due to the presence of different mantle minerals (MgO vs. Mg_2SiO_4, $MgSiO_3$). The experiments with T-cup, performed at 16 GPa, also show similar

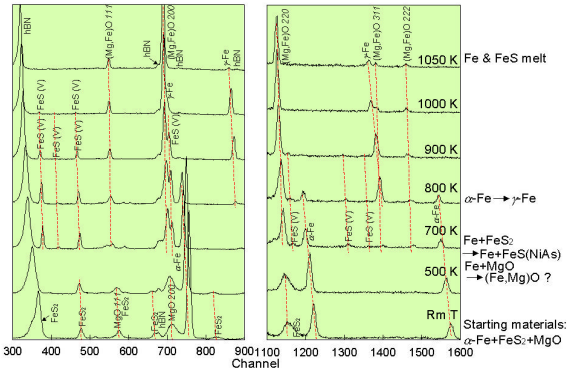

FIG. 2. X-ray diffraction change during heating cycle for the system Fe-FeS_2-MgO. Pyrite FeS_2 starts reacting with Fe at 700K. At the same time, both MgO and Fe (with bcc structure) peaks drift toward low energy, indicating the expansion of lattice parameters with the same structure. Then a-Fe transforms to g (fcc) phase at 800K. Above 1000K, both Fe and FeS (with NiAs structure) disappeared, meaning these materials melt.

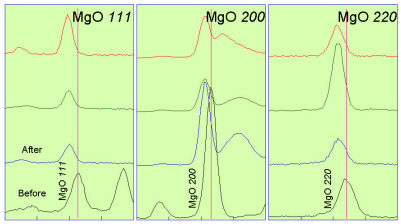

FIG. 3. Comparison of x-ray diffraction patterns at ambient conditions for the system Fe-FeS_2-MgO. The bottom line shows the diffraction pattern before the experiment. The top three lines, whose data were collected at different positions in the sample, show the pattern after the experiment. The MgO peaks are significantly shifted toward lower energy.

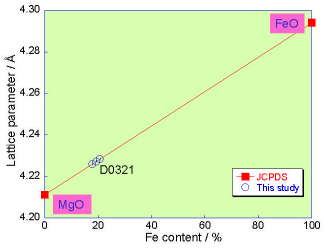

Fig. 4. Lattice parameter of magnesiowüstite as a function of Fe content. From the peak shift of MgO, shown in Fig. 3, we can estimate the Fe content, if it is assumed there is a linear relation between the lattice parameter and Fe content. The Fe content of this run was estimated to be about 20% in molar ratio.

results; the only difference from the DIA runs is that Fe transforms to the *e* phase (hexagonal close-packed [hcp] structure), which then reacts with FeS_2 before melting. In these T-cup runs, MgO shows a significant peak shift, while Mg_2SiO_4 and $MgSiO_3$ do not. Diffraction patterns collected at ambient conditions after the runs, shown in Fig. 8, are consistent with those of the DIA runs. Other preliminary experiments — which used commercial FeS (not pure troilite but troilite containing free Fe and S) as the sulfur source instead of pyrite FeS_2 and used the same sample container materials (a mixture of amorphous boron and epoxy, BN, or MgO) — showed the same feature as well.

Critically speaking, the oxidation state (oxygen fugacity) could be different depending on the nature of the sample container and *P-T* path; however, if free oxygen is the critical ingredient for the reaction between Fe and MgO, we should observe FeO in the systems containing $MgSiO_3$ and Mg_2SiO_4 as well as the system containing MgO because there is no other difference except for the sample itself. Chemical analysis has not been performed, so the main reason of the peak shifts has

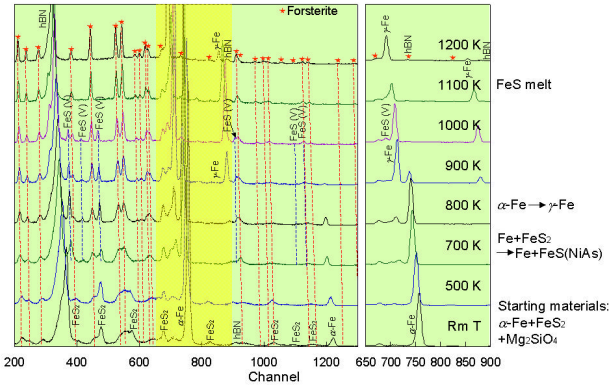

FIG. 5. X-ray diffraction change for the system Fe-FeS_2-Mg_2SiO_4 during heating. Mg_2SiO_4 peaks, marked by stars, remain unshifted more than thermal expansion, even when FeS_2 reacts with Fe, forming FeS (NiAs structure), and Fe transforms to g phase.

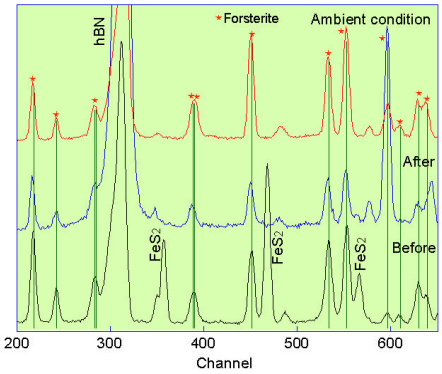

FIG. 6. Comparison of x-ray diffraction patterns at ambient conditions for the system Fe-FeS_2-Mg_2SiO_4. Bottom line shows the diffraction pattern before the experiment. The top two lines collected at different sample positions show the pattern after the experiment. The Mg_2SiO_4 peaks went back to the original position, while the FeS_2 peaks are lost by the formation of FeS, which is identified as troilite.

not yet been fully addressed. Nevertheless, this observation, combined with tomography results, could be an important clue. If the iron (sulfide) reacts with a mantle mineral, surface tension is dramatically reduced, and, as a result, iron-dominant melt spheres cannot be formed. If the iron (or iron sulfide) does not react with the surrounding mineral, then surface tension remains high, allowing iron droplets to form.

On the basis of the assumption that a certain amount of sulfur exists in the Earth, if the segregation process starts at low pressure (below 24 GPa), there will be very little MgO in the mantle to react with the Fe-rich melt, and thus

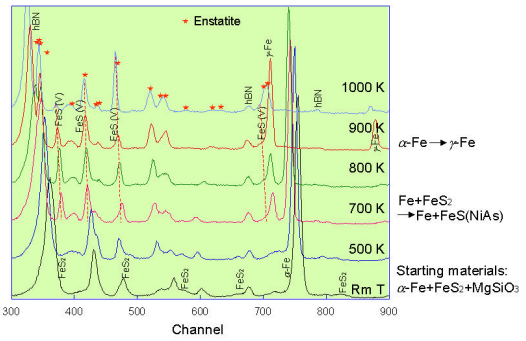

FIG. 7. X-ray diffraction change for the system Fe-FeS_2-$MgSiO_3$ while the sample is heated. Enstatite $MgSiO_3$ is inert for both Fe and FeS.

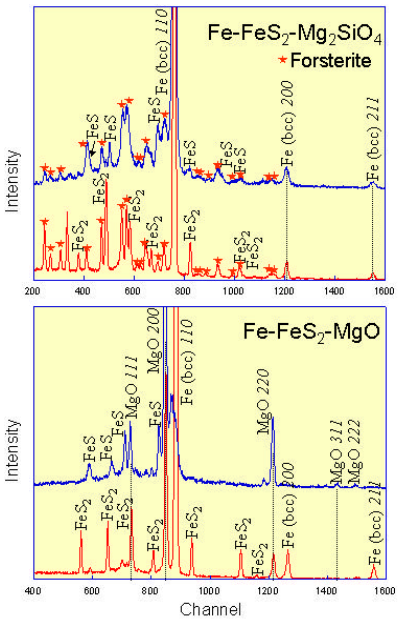

FIG. 8. Comparison of x-ray diffraction patterns at ambient conditions for the systems containing Mg_2SiO_4 and MgO recovered from T-cup runs that performed at 16 GPa. In the system containing MgO, both Fe and MgO peaks shifted toward low energy; in the system involving Mg_2SiO_4,, the Mg_2SiO_4 peaks remained unshifted. Although the pressure range in which the experiments were performed was quite different, the results are consistent with DIA runs.

the segregation process can proceed without difficulties. Certain giant impact models propose that the moon is a "by-product" formed from a half-sized Earth and a Mars-sized protoplanet. Since the moon has a very small core, the Earth's core formation should have been almost done by the time the giant impact occurred [7, 8]. Although the pressure at the center of the half-sized Earth is unknown,

it should be much smaller than that of current Earth. This giant impact model does not conflict with the segregation of Fe-rich melt. and sulfur could exist in the core. Our observation may "act in reverse" toward inferring the scale of the Earth during the segregation.

The recent giant impact model reported by Canup and Asphaug [9] prefers a full-formed rather than a half-formed Earth. This model increases the pressure range in which core formation happened. Even if the segregation happens under upper mantle conditions, the Fe-rich melt reacts with MgO during the migration process through the lower mantle, and, depending on the dynamics, either the Fe melt is completely consumed before it reaches the center of the Earth, or the Fe-rich core is in significant disequilibrium with the lower mantle. From the geological timescale, however, such significant disequilibrium is difficult to justify. As a result, sulfur may be eliminated from being a candidate as one of the light element(s) in the core, since our observation indicates that iron sulfide cannot migrate through the lower mantle by the reaction, while the Earth's core exists right now.

Acknowledgments

We thank N. Lazarz, F. Sopron, M. Jagger, G. Shen, M. Newville, P. Eng, J. Pluth, P. Murray, C. Pullins, L. Gubenko, and P. Dell for their valuable contributions. Work performed at GSECARS is supported by the National Science Foundation (Earth Sciences), U.S. Department of Energy (DOE, Geosciences), W. M. Keck Foundation, and U.S. Department of Agriculture. Use of the APS was supported by the DOE Office of Science, Office of Basic Energy Sciences, under Contract No. W-31-109-ENG-38.

References

[1] A. M. Dziewonski and D. L. Anderson, Phys. Earth Planet. Inter. **25**, 297-356 (1981).
[2] F. Birch, J. Geophys. Res. **57**, 227-286 (1952).
[3] F. Birch, J. Geophys. Res. **69**, 4377-4388 (1964).
[4] A. P. Jephcoat and P. Olsen, Nature **325**, 332-335, (1987).
[5] T. Uchida, Y. Wang, M. L. Rivers, and S. R. Sutton, J. Geophys. Res. **106**, 21799-21810 (2001).
[6] J.-P. Poirier, Phys. Earth Planet. Inter. **85**, 319-337 (1994).
[7] A. G. W. Cameron and W. R. Ward, Lunar Sci. **7**, 120-122 (1976).
[8] W. K. Hartmann and D. R. Devis, Icarus **24**, 504-515 (1975).
[9] R. M. Canup and E. Asphaug, Nature **412**, 708-712 (2001).